


S. WITTE
R.T. ZINKSTOK
W. HOGERVORST
K.S.E. EIKEMA 

Numerical simulations for performance optimization of a few-cycle terawatt NOPCPA system

Atomic, Molecular and Laser Physics Group, Laser Centre Vrije Universiteit, De Boelelaan 1081, 1081 HV Amsterdam, The Netherlands

Received: 1 December 2006/Revised version: 14 March 2007
Published online: 16 May 2007 • © Springer-Verlag 2007

ABSTRACT We present a systematic numerical design and performance study of an ultra-broadband noncollinear optical parametric chirped pulse amplification (NOPCPA) system. Using a split-step Fourier approach, we model a three-stage amplifier system which is designed for the generation of 7 fs pulses with multi-terawatt peak intensity. The numerical results are compared with recent experimental data. Several important aspects and design parameters specific to NOPCPA are identified, and the values of these parameters required to achieve optimal working conditions are investigated. We identify and analyze wavelength-dependent gain saturation effects, which are specific to NOPCPA and have a strong influence on the parametric amplification process.

PACS 42.65.Yj; 42.65.Re

1 Introduction

Noncollinear optical parametric chirped pulse amplification (NOPCPA) has attracted a lot of attention recently because of its potential as a source of few-cycle laser pulses with peak intensities exceeding a terawatt [1]. Such high-intensity ultrashort pulses have many applications in the field of strong-field physics [2], e.g., as a driver source for the generation of single attosecond pulses at extreme-ultraviolet wavelengths [3], or for relativistic optics in the few-cycle pulse regime [4]. In addition, laser-based particle accelerators using few-cycle pulses have recently become the subject of investigation [5].

Therefore, it is not surprising that research on NOPCPA has been expanding rapidly in the last few years, with many demonstrations of new NOPCPA implementations at various wavelengths, repetition rates and intensities. This progress has led, for example, to the first demonstration of sub-10-fs pulses with a peak intensity exceeding one terawatt [6] and to the development of a table-top laser system delivering 45 fs pulses with 200 TW peak intensity [7]. Carrier-envelope phase-stable NOPCPA systems have already been constructed for lower peak intensities [8, 9]. Recently, we have demon-

strated an NOPCPA system which produces near-Fourier-limited 7.6 fs pulses with a peak intensity of 2 TW running at a 30 Hz repetition rate [10]. This system also proved that NOPCPA can be used to amplify pulses with very low levels of parametric fluorescence (less than 0.2% of the total integrated energy), and a pre-pulse contrast of 10^{-8} was achieved. Besides producing the shortest terawatt-intensity pulses ever achieved with the NOPCPA technique (only 2.7 optical cycles), this system approaches the theoretical limits that can be expected from such a 532 nm pumped BBO-based NOPCPA system [1, 11].

The theoretical basis for NOPCPA has its origin in the well-known process of optical parametric amplification and is therefore well established [1, 11–13]. However, the theoretical research and numerical simulations specific to NOPCPA that have been published all seem to focus almost exclusively on the achievable power and gain bandwidth by exploring different types of phase-matching geometries [14–16]. Although this has led to designs for ultrashort pulse petawatt amplifier systems [11] and ultra-broadband phase-matching geometries using angular dispersion [17, 18], hardly any study seems to have been performed from a more experimental point of view. With the exception of a recent numerical study on the pulse contrast [19], a systematic study which models a realistic NOPCPA setup aimed at identifying optimum values and finding stability requirements for important experimental parameters has – to the best of the authors' knowledge – not been published to date.

In this paper, we present numerical simulations on a three-stage NOPCPA system designed for the amplification of few-cycle pulses to multi-TW peak intensity. The numerical results are used to interpret recently obtained experimental data [10], and several key parameters are systematically varied to obtain information on how to optimize NOPCPA performance. From the numerical data, interesting conclusions can be drawn about the NOPCPA process, and an outlook is given on possible further improvements that can be applied to present experimental systems.

2 Numerical modeling of NOPCPA

In order to describe the optical parametric amplification process, we write the coupled-wave equations for the slowly-varying electric field pulse envelopes A_m (where

 E-mail: kse.eikema@few.vu.nl

$m = s, i, p$ indicate signal, idler and pump respectively), restricting ourselves to one-dimensional propagation and neglecting walk-off effects (see e.g. [20]):

$$\frac{\partial A_s}{\partial z} + \sum_{n=1}^{\infty} \frac{(-i)^{n-1}}{n!} k^{(n)} \frac{\partial^n A_s}{\partial t^n} = -i \frac{\chi^{(2)} \omega_s}{2n_s c} A_p A_i^* e^{-i\Delta k \cdot z} \quad (1a)$$

$$\frac{\partial A_i}{\partial z} + \sum_{n=1}^{\infty} \frac{(-i)^{n-1}}{n!} k^{(n)} \frac{\partial^n A_i}{\partial t^n} = -i \frac{\chi^{(2)} \omega_i}{2n_i c} A_p A_s^* e^{-i\Delta k \cdot z} \quad (1b)$$

$$\frac{\partial A_p}{\partial z} + \sum_{n=1}^{\infty} \frac{(-i)^{n-1}}{n!} k^{(n)} \frac{\partial^n A_p}{\partial t^n} = -i \frac{\chi^{(2)} \omega_p}{2n_p c} A_s A_i e^{i\Delta k \cdot z} \quad (1c)$$

where $k^{(n)}$ is the n^{th} order dispersion coefficient, and $\Delta k = k_p - k_s - k_i$ is the magnitude of the wave-vector mismatch. It should be noted that in these one-dimensional equations $e^{i\Delta k \cdot z}$ contains the scalar product of the vectors $\Delta \mathbf{k}$ and \mathbf{z} . The assumption that walk-off can be neglected is justified by the relatively large beam sizes used in the interaction (~ 2 mm in the first two passes, and 10 mm in the last pass). In addition, in this particular noncollinear geometry, the walk-off angle of the pump beam is close to the noncollinear angle that is used, so that the effective interaction length is hardly affected. Although analytical solutions exist in terms of Jacobi elliptic integrals if the effects of dispersion are ignored, we employ a split-step Fourier algorithm [21] to find numerical solutions to the full set of coupled-wave equations without the need for such an assumption. In this type of algorithm the interaction medium is divided into a number of small slices. For every step, the equations are first solved in the time domain using only the nonlinear source terms. The obtained solution is then Fourier-transformed into the frequency domain where the step through the crystal is taken again, this time using only the dispersive terms in (1c). The resulting pulse envelopes are inverse Fourier-transformed back to the time domain, where the next nonlinear step is taken, and so forth. The advantage of this algorithm is that it includes dispersion to all orders simply by multiplying every frequency component with a phase shift determined from the traversed path length and the refractive index as obtained from the Sellmeier equations. In this way, the full series expansion for the dispersion in (1c) is taken into account, simply by Fourier transformation, multiplication, and inverse Fourier transformation back to the time domain. The nonlinear step is taken by integrating (1c) using a fourth-order Runge–Kutta solver with adaptive stepsize control [22].

The algorithm requires the electric field envelopes of a pump and a seed pulse in the time domain as input data. It starts out by solving the six coupled-wave equations for all real and imaginary parts of pump, seed and idler pulses. In this integration, the phase-mismatch term $e^{i\Delta k \cdot z}$ for the carrier frequencies in (1c) has been incorporated into the pulse envelopes $A_m(z, t)$; in this way, the phase mismatch between the waves is introduced in a natural way through the dispersive propagation step. The number of slices needed to achieve sufficient accuracy is determined by repeating a simulation using typical input data with an increasing number of slices, until the solution converges. The propagation step is calculated in the reference frame of the pump pulse. This is done for convenience, as the time axis can be kept smaller in this frame.

The numerical model describes a three-stage amplifier similar to the experimental system presented in [10]. This system employs 5 mm long BBO crystals cut for type-I phase matching, pumped by a 60 ps frequency-doubled Nd:YAG laser system at 532 nm. In this amplifier, the first two passes are pumped by 10 mJ pulses. After this pre-amplifier stage, the amplified signal beam is expanded from 2 to 10 mm diameter by a telescope and sent to a third amplification pass pumped by 150 mJ pulses. In our model, we have used the Sellmeier equations for BBO as given by Zhang et al. [23]. The nonlinear susceptibility $\chi^{(2)}$ of BBO has been taken to be 4.0×10^{-12} m/V. Typically, the simulations are performed using pump intensities ~ 7.5 GW/cm² in the first two passes and ~ 6 GW/cm² in the last pass, and an input pulse energy of ~ 1 nJ. These model pump intensities have been used because they lead to the best match between the calculated spectra and the experimental observations. While the intensity of the first passes corresponds well to the estimated experimental value, the intensity of the last pass is about 20%–50% higher than expected. This is probably due to uncertainties in the exact pump pulse shape and duration, and to several other experimental parameters that influence the interaction in the last crystal. The effect of higher-order nonlinearities on the parametric interaction has been neglected, which is justified since the total integrated nonlinear phase shift (known as the B-integral) of our NOPCPA system is estimated to be only 0.37 rad at maximum intensity.

3 Optimization of spectral bandwidth

Both the gain and bandwidth of the amplifier system depend sensitively on the phase matching conditions. The strong effect of the phase mismatch on the parametric amplification process is explained by the different frequency-dependent nonlinear propagation characteristics of the various pulses. This can be seen explicitly from the complex $e^{i\Delta k \cdot z}$ -term in the nonlinear polarization of the coupled-wave (1c), which splits into an imaginary part that causes a phase shift between waves, and a real part that directly influences the gain. Therefore, many characteristics of an NOPCPA system can already be predicted by the shape and size of the phase-mismatch curve as a function of wavelength.

The phase-matching conditions are largely determined by two angles (see Fig. 1). These are the phase-matching angle θ between the optical axis of the crystal and the wave-vector of the pump beam, and the noncollinear angle α between the pump and signal wave-vectors inside the crystal. The major influence that these angles have on the parametric amplification process is demonstrated by performing simulations using different values for these angles, as shown in Fig. 2. The central values for the angles in this simulation are $\theta = 23.829^\circ$ and $\alpha = 2.36^\circ$, which are close to the optimum values for broadband phase matching [11, 24], as is also confirmed by the present calculations. The effect of adding slight variations $\Delta\theta$ (where in this case $\Delta\theta = \pm 0.06^\circ$) to θ is shown in the left panels of Fig. 2: Changing θ has the effect of shifting the phase-mismatch curve up or down in a wavelength-independent way, and consequently the gain is seen to be highest in the regions where the phase-mismatch is minimized. Figure 2b demonstrates the effect of changing α , which

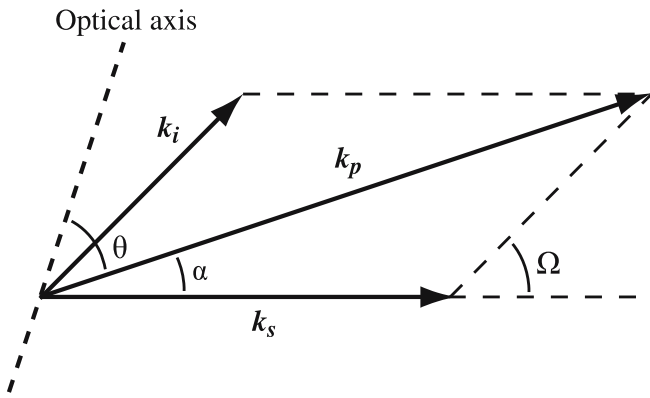


FIGURE 1 Phase-matching geometry for noncollinear optical parametric amplification

is to tilt the phase-mismatch curve, allowing it to be minimized over a large spectral bandwidth. In these simulations, θ was adjusted such that the phase-mismatch at 800 nm is zero, so that the phase mismatch curve is effectively tilted around this center wavelength. While an angle $\alpha = 2.36^\circ$ leads to a very broad amplified spectrum with some modulation, the amplified bandwidth can be made even broader by tuning α to slightly smaller values. However, this is only achieved at the cost of stronger spectral intensity modulations. The reason for this is immediately apparent from the phase-mismatch curves, which are tilted from a monotonously decreasing function at large α to a shape with local maxima and minima at smaller α . This phase-mismatch curve at small α contains three zero-crossings, leading to the three-peak structure of the spectrum. Between these zero-crossings the phase excursions become quite substantial, causing a strong suppression of the gain at these wavelengths. From an experimental point of view, Fig. 2 demonstrates the high accuracy with which θ and α need to be set, as changes on the order

of 0.01° already have a significant effect on the amplification process.

4 Modeling an experimental NOPCPA system

The usefulness of a numerical model is of course determined by its ability to simulate the behavior of a realistic experimental system. Therefore, we initially tested the ability of the numerical algorithm to reproduce the output characteristics of our experimental NOPCPA system from its input parameters. For all the simulations described in this paper, we used pump and seed pulse durations that correspond to our experimental situation [10]. Specifically, we have used transform-limited 60 ps pump pulses with a Gaussian temporal and spectral shape, with a central wavelength of 532 nm. However, in the experiment the angles θ and α in each pass are optimized for optimal broadband amplification, but their exact values are not known to the required level of accuracy in order to simply insert them into the model. The same problem arises for the exact pump-seed timing delay for each pass. Therefore, to find a spectrum that matches the experimental data, we performed a series of simulations for varying sets of noncollinear angles and phase mismatches. Due to the large parameter space and to save computation time, we restricted the search by using the same noncollinear angle and phase mismatch in all three amplification passes.

A comparison between the measured spectrum and a model calculation is shown in Fig. 3. This simulation is performed using a noncollinear angle α of 2.31° and a phase-matching angle θ of 23.783° in all crystals. The shape of the simulated spectrum corresponds very well to the experiment and all the general features are reproduced. Some discrepancies are visible, such as the shift in the position of the peak structure around 730 nm to shorter wavelengths, and the relatively sharp edge around 860 nm, which is smoother in the simu-

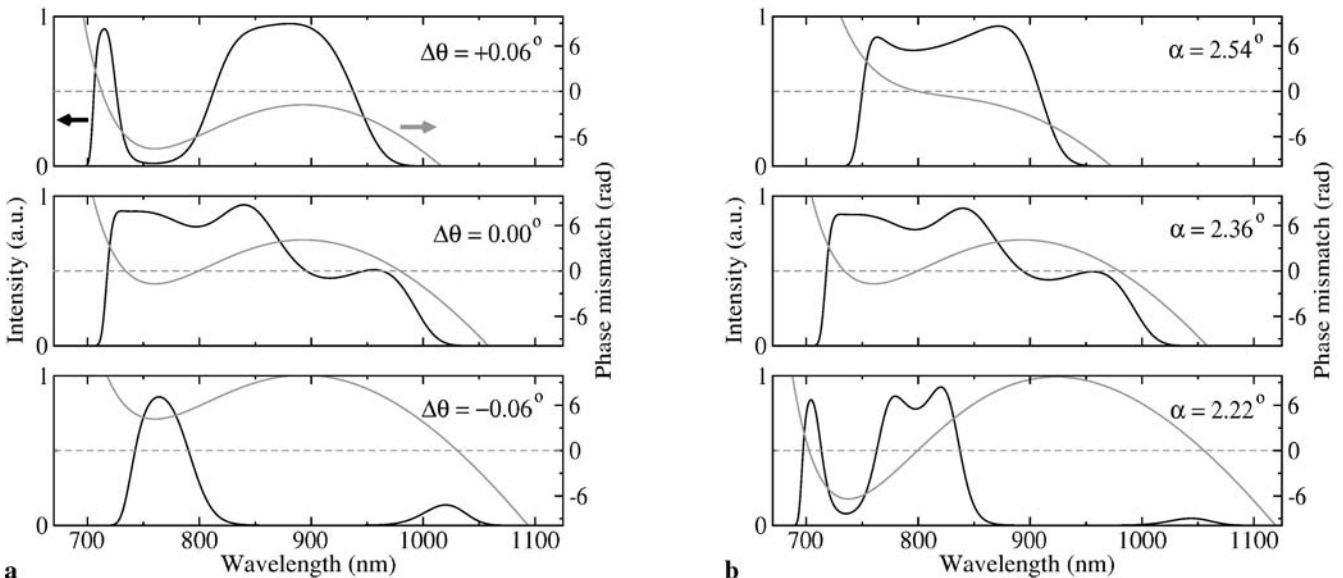


FIGURE 2 Numerical simulations of the wavelength-dependent output of a three-stage NOPCPA system. (a) Using various phase-matching angles $\theta = 23.829^\circ + \Delta\theta$, while keeping $\alpha = 2.36^\circ$. (b) Using various noncollinear angles α , while adjusting θ to optimize phase-matching at a wavelength of 800 nm. The *black lines* represent the amplified signal spectra, while the *grey lines* are the corresponding wavelength-dependent phase mismatches. The *dashed grey lines* indicate zero phase mismatch

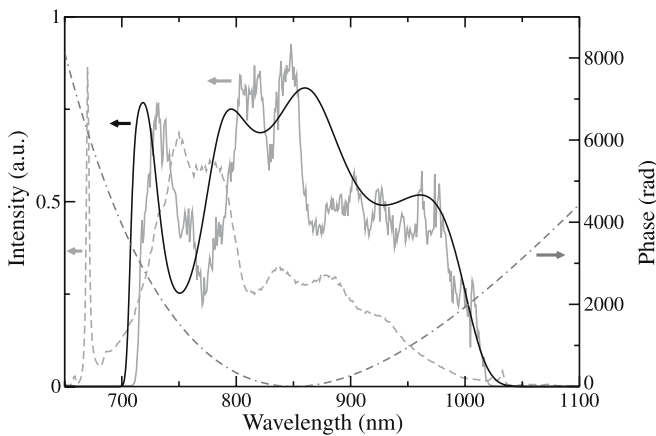


FIGURE 3 Comparison of a measured output spectrum from our NOPCPA system (*grey trace*) with a numerical simulation (*black trace*). A relatively straightforward calculation already reproduces the main features of the spectrum, although the exact wavelengths at which they occur are slightly shifted. The *dashed grey trace* is the input seed spectrum, and the *dash-dotted dark grey line* is the phase of the amplified seed pulse. The Fourier-limited pulse durations are 7.1 fs for the simulated spectrum, 7.3 fs for the experimental amplified spectrum, and 6.2 fs for the input seed spectrum, respectively. See text for details

lation than in the experimental spectrum. These details are most likely caused by slight variations in angles and pulse timings between amplification passes. However, aside from these small differences, a good agreement is found between numerical simulation and experimental observation, which assures that the model is capable of making realistic predictions of the output characteristics of our NOPCPA system. The amplified pulses have a well-behaved spectral phase, and can therefore be recompressed close to their Fourier-limited pulse duration, as we have already demonstrated experimentally [10]. Because of the large spectral bandwidth of the pulses, we employed adaptive phase-shaping using a spatial

light modulator to compensate the higher-order dispersion terms.

A convenient feature of the split-step algorithm is that the pulse shapes and spectra of all three involved waves are calculated in small steps through each crystal, and the data from each of these steps can be saved individually. The amplification process is, thus, automatically monitored at various positions inside the crystal, as shown in Fig. 4. In Fig. 4a the temporal pulse profile of the signal is plotted as it travels through the first crystal, while Fig. 4b displays the signal spectrum as the pulse propagates through the last crystal. From these pictures, the pulse evolution in the entire amplifier can be studied in both frequency- and time domain.

5 Wavelength-dependent gain saturation

An interesting feature of NOPCPA is depicted in Fig. 5, which consists of cuts through the data of Fig. 4b taken at various wavelengths. This graph reveals the wavelength-dependent gain dynamics as the amplification process saturates in the last crystal. While the wavelengths with the highest gain (i.e. the lowest phase mismatch) already saturate and even exhibit energy back-conversion, wavelengths with a lower gain still display a small-signal exponential gain behavior. This effect does not occur in conventional (e.g. Ti:Sapphire) amplifiers, and is directly related to the instantaneous nature of parametric amplification. Since the seed pulse is chirped, its frequency components are separated in time and overlap with different parts of the pump pulse. Therefore, each wavelength has its own “slice” of pump light available for amplification, without competition from the other wavelengths. The interaction length that is required for gain saturation then depends only on the phase mismatch for this particular wavelength, leading to the behavior that is observed in Fig. 5. The small dip around 820 nm in the amplified spectrum shown in

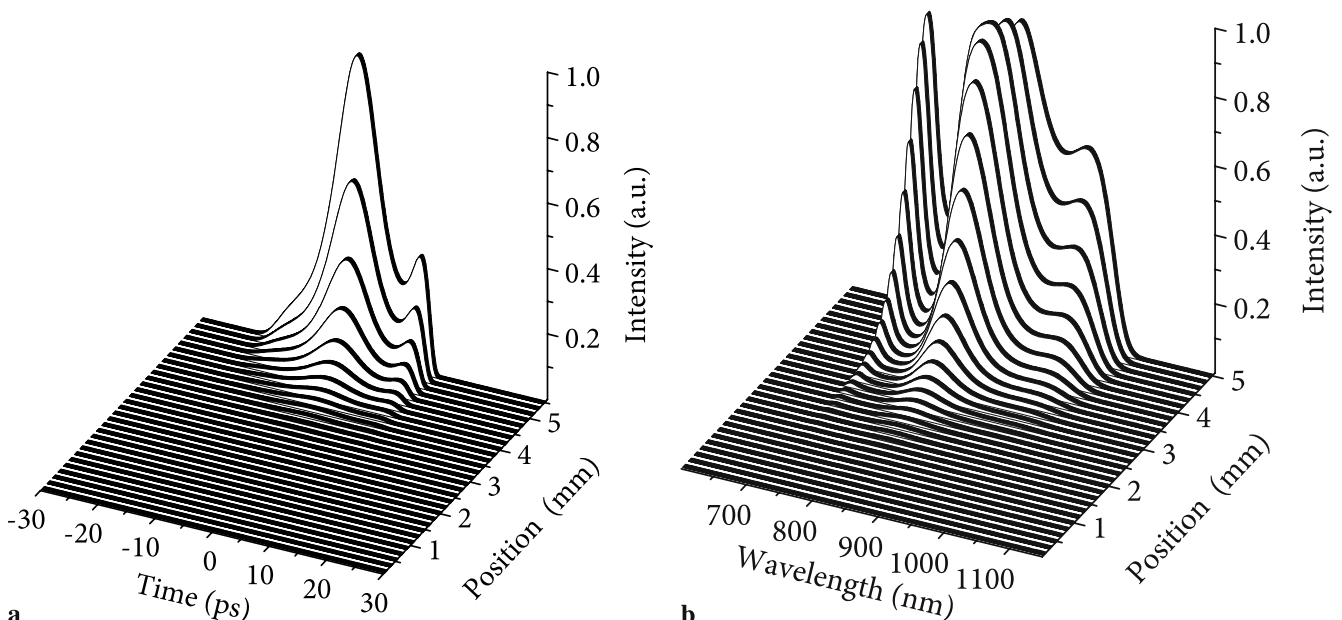


FIGURE 4 (a) Temporal profile of the signal pulse during amplification in the first pass. (b) Spectral amplitude of the signal pulse in the last amplification pass

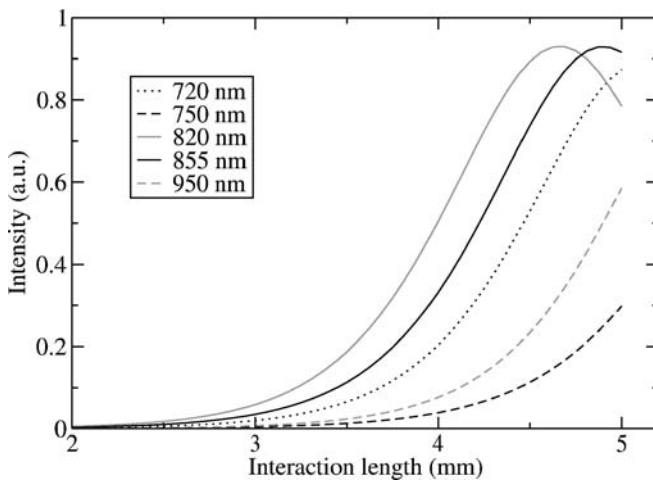


FIGURE 5 Wavelength-dependent gain saturation: Due to the differences in phase mismatch, the NOPCPA gain is frequency-dependent. Since all the frequencies are temporally separated in the chirped seed pulse, gain saturation and even backconversion independently occurs for every wavelength

Fig. 3 may be explained by such spectrally dependent amplification dynamics, as the simulation indicates some energy back-conversion to occur at this wavelength. In a configuration where the gain is even higher, this effect can lead to an increasingly complicated spectral structure with various peaks and dips depending on the saturation regime experienced by each spectral component. From an experimentalist's point of view, the occurrence of wavelength-dependent gain saturation calls for a high pump pulse intensity stability because a change in pump power affects all the spectral components of the signal pulse in a different way. For example, by analyzing the saturation curves shown in Fig. 5 it can be seen that a decrease in pump intensity leads to a stronger signal intensity decrease at 950 nm than at 855 nm, while at the same time the intensity at 820 nm would increase. Such spectral variations directly translate into changes of the temporal pulse shape, causing undesirable intensity-dependent changes of the pulse duration. To assess the magnitude of this effect, we have repeated the simulations that resulted in Fig. 5 using different pump intensities. For a pump intensity variation of 4%, the transform-limited amplified seed pulse duration is found to change by $\sim 5\%$. In addition, we have measured the output spectrum of our NOPCPA system [10] at various power levels and found similar results. Such coupling between pump intensity fluctuations and the shape of the final spectrum will become more pronounced when the total gain of the amplifier increases. As a result, a high intensity stability of the pump laser is essential for reliable NOPCPA operation.

Another important consequence of wavelength-dependent gain saturation is that the beam profile of the pump laser system should be very homogeneous. From the discussion in the previous paragraph, it is clear that any pump intensity variation will lead to a different amplified spectrum, and therefore to a different amplified pulse duration. Therefore, any spatial intensity variations across the pump beam profile will also translate into spatial variations of the amplified spectrum and pulse duration. A direct consequence is that the pump pulse of a few-cycle NOPCPA system needs to be top-hat shaped, to prevent a spatially dependent pulse duration after amplifi-

cation. In addition, temporal fluctuations of the pump beam profile should be avoided.

An estimate of the total pump-to-signal conversion efficiency for a specific set of parameters can be obtained by looking at the pulses in the time domain, as shown in Fig. 6. This figure demonstrates that the present NOPCPA configuration already operates with strong local pump depletion. From calculations by Ross et al. [11], it is known that in principle, 100% conversion efficiency is possible when the phase-mismatch Δk is zero and group velocity effects are absent. The presence of a nonzero Δk and the occurrence of a small group velocity mismatch, therefore, place a limit on the maximum efficiency. In addition, the interaction length needed to achieve maximum conversion becomes longer when $\Delta k \neq 0$. Our simulations show that with the present experimental parameters we can achieve $> 90\%$ conversion at wavelengths where the phase mismatch is minimized. However, since the signal pulse has been chosen shorter than the pump pulse to efficiently amplify all spectral components, the total conversion efficiency is much lower. For the amplified pulses shown in Fig. 6, the pump-to-signal energy conversion efficiency is 17%, while the idler then takes another 8.5% of the initial pump energy. This number is quite close to the experimentally achieved pump-to-signal conversion efficiency of about 19%.

From Fig. 6 it can be seen that during amplification the shape of the signal pulse has changed from a Gaussian input pulse to a strongly modulated square-like structure. This is also the result of the instantaneous wavelength-dependent amplification process which leads to a temporal pulse shape that mimics the shape of the amplified spectrum. Note that for a positively chirped pulse the shortest wavelengths are at the trailing edge of the pulse, which is confirmed by comparing the structure of the signal pulse in the time-domain picture in Fig. 6 with the corresponding frequency spectrum in Fig. 3. This behavior can already be seen before saturation sets in, as is shown in Fig. 4a, where the wavelength-dependent differences in gain lead to a reshaping of the amplified seed pulse. Again, this is a feature specific to NOPCPA which is not encountered in amplifier systems that use energy storage in a medium, such as Ti:Sapphire. This feature opens up the

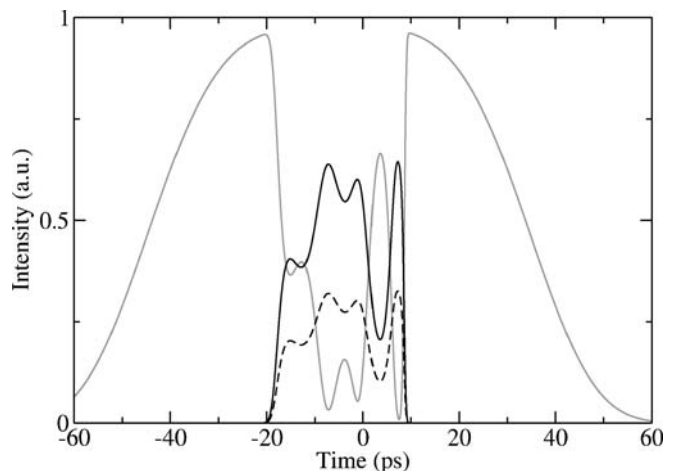


FIGURE 6 Temporal profile of pump (grey curve), signal (black curve) and idler (dashed curve) after amplification. The total pump-to-signal energy conversion is about 17%, although local pump depletion exceeds 90%

possibility of spectral amplitude shaping by using a temporally modulated pump pulse, which also makes it possible to control the shape of the Fourier-limited pulse shape of the final amplified output pulse in the time domain. However, it also causes the transfer of noise which may be present on the pump pulse profile (due to e.g. mode-beating in a system based on a multimode pump laser) to the spectral shape of the amplified signal pulse [25].

6 Pump-seed synchronization

The duration of pump and seed pulses and the timing between them can have a significant influence on the parametric amplification process because of the instantaneous nature of the interaction. Intuitively it is to be expected that timing fluctuations on the order of the pump pulse duration will cause significant changes in the amplified spectrum. Also, the ratio between pump and seed pulse durations is expected to be an important parameter in the case of Gaussian pump pulses. For instance, when the seed pulse is much shorter than the pump pulse, the amplification will be inefficient. However, if the seed pulse is chirped too strongly, only its central part will be amplified, leading to a narrowed spectrum. When the exact pulse shape of the pump pulse is also taken into account, it is clear that the final output spectrum depends heavily on the pulse overlap and there is a tradeoff between bandwidth and efficiency, especially for ultra-broadband few-cycle seed pulses.

To determine the influence of the pump-seed timing, we measured the spectrum from our NOPCPA system at various pump-seed delays using a translation stage to introduce a controlled delay of the seed pulse. In our experimental situation, the pump-seed timing can be stabilized with a residual jitter well below 1 ps [9]. The results of these measurements are shown in Fig. 7. In general, a good agreement between

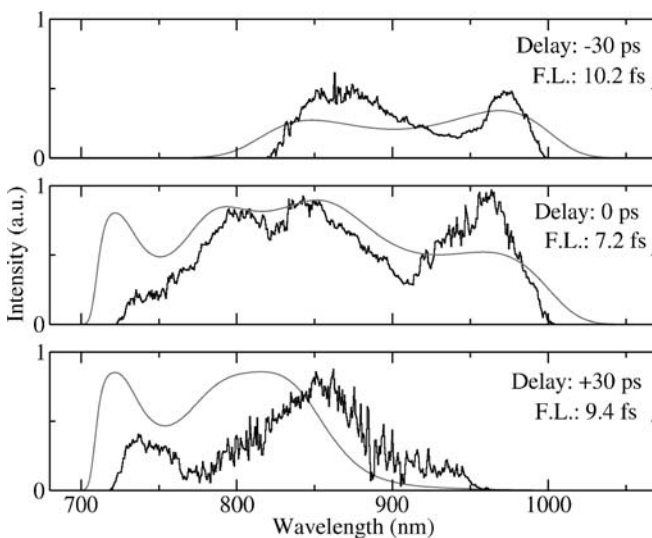


FIGURE 7 Comparison between simulations (grey traces) and experiment (black traces) of the influence of the pump-seed timing delay on the amplification process: A reasonably good agreement is obtained, although the shape of the spectrum at a given delay depends on the exact pump pulse shape and the relative delays between different amplification passes. The pump-seed delay and Fourier-limited pulse duration are given in each graph

the numerical simulations and the experiment is obtained, although the measurements have been carried out with a spectral gain bandwidth which was not fully optimized. The measured spectra show the same timing dependence as has been predicted by the model, although the exact shape of the spectra differs somewhat from the model calculations. This is mostly due to some residual timing differences between the various amplification passes, leading to a slightly different influence on each pass. The exact shape of the pump pulse is also of considerable influence, especially at larger delays where saturation is less prominent.

To find the optimum value for the ratio between the durations of the pump and chirped seed pulses, simulations have been performed using various amounts of group velocity dispersion for the input seed pulse. The results are shown in Fig. 8. As expected, a small group velocity dispersion (i.e., a short pulse) leads to a broad amplified spectrum with a relatively low intensity. When the chirp increases the pump-seed overlap improves, resulting in a rapid increase in efficiency. However, the spectrum is also observed to narrow down as the chirp increases since the spectral wings (which are on the

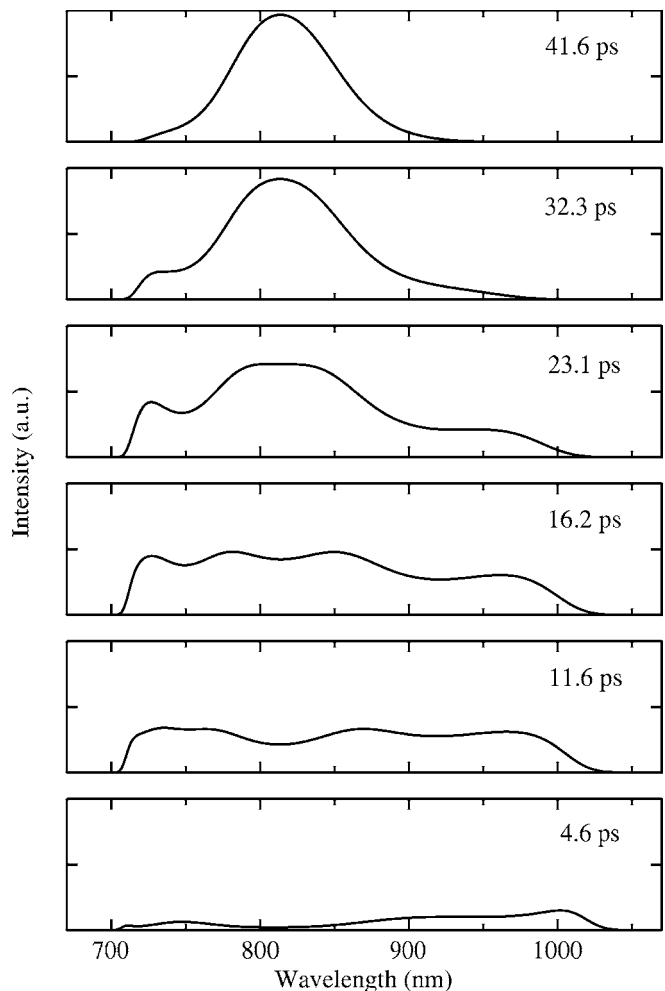


FIGURE 8 Simulation of a three-stage NOPCPA system for different amounts of group velocity dispersion on the input seed pulse: Pulses with a larger chirp amplify more efficiently, but only at the cost of a reduced spectral bandwidth. The pump pulse FWHM duration is 60 ps; the FWHM pulse duration of the stretched seed pulse is given in each graph

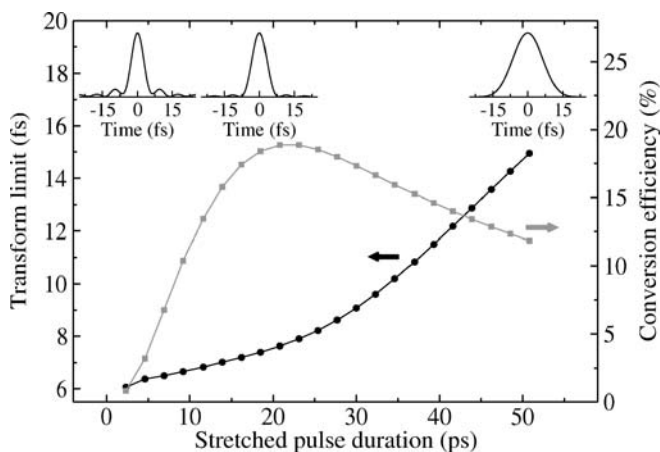


FIGURE 9 The transform-limited pulse duration of the amplified pulses (black circles) and the pump-to-signal conversion efficiency (grey squares) as a function of the stretched seed pulse duration, for the case of 60 ps Gaussian pump pulses. The transform-limited pulse shapes that are shown correspond to a seed pulse duration of 2.3 ps, 16.2 ps and 50.8 ps, respectively

edges of the chirped pulse) now overlap with a lower-intensity part of the pump pulse. This tradeoff between spectral bandwidth and conversion efficiency has been depicted graphically in Fig. 9 together with the transform-limited pulse shapes for three different stretched pulse durations. The square shape of the amplified spectrum at low chirp values leads to some side-lobes on the transform-limited pulse shape. From Fig. 9, it is clear that when using Gaussian-shaped pump pulses, the maximum conversion efficiency can only be reached at the cost of the shortest achievable amplified pulse duration. For the highest chirp values, even the total efficiency goes down. The reason for this is that the large stretching ratio lowers the input seed intensity to a point where the amplifier no longer saturates properly. From the simulations shown in Fig. 8, we can conclude that the seed pulse should be stretched to about 0.2–0.3 times the pump pulse duration for a good balance between spectral bandwidth and conversion efficiency. A higher conversion efficiency can be achieved, but only at the expense of the amplified bandwidth. Note that a maximum efficiency can be obtained if the pump pulse has a square temporal shape because all the spectral components in the chirped seed pulse then experience the same gain, and the ratio between the pulse durations can, in principle, be set to one [26]. The generation of such a square pulse shape, however, is not trivial for the case of picosecond pump pulses.

7 Conclusion

In conclusion, we have performed numerical simulations of a terawatt-class few-cycle NOPCPA system consisting of three amplification stages. The results show good agreement with experimental data from the 2 TW, 7.6 fs NOPCPA system that we recently developed in our laboratory [10]. As a result, we can take advantage of this model to predict the behavior of our NOPCPA system under various operating conditions and analyze the influence of important parameters on the amplification process.

By following the evolution of the amplified seed pulse intensity in both time and frequency domains, we observe

and analyze wavelength-dependent gain saturation, which is a phenomenon that is caused by the instantaneous nature of the amplification process and is, therefore, specific to NOPCPA. This effect places stringent requirements on the pump intensity stability to prevent intensity-dependent fluctuations of the amplified pulse duration. From our calculations, we find that a 4% pump intensity jitter translates into a 5% variation of the Fourier-limited amplified pulse duration.

We have used the numerical model to find optimized values for the phase-matching- and noncollinear angles, and to study the effects of timing jitter between the pump and seed pulses. Also, we investigated the influence of the stretching factor of the seed pulse on the amplification process and found a good compromise between amplified bandwidth and efficiency when the seed pulse is stretched to a value around 0.2–0.3 times the pump pulse duration (in the case of Gaussian temporal profiles). The model calculations presented here provide a realistic picture of the operating conditions of our experimental NOPCPA system. Therefore, this numerical approach can be used to design future implementations of more advanced amplifier systems with a more complicated geometry and, therefore, aid in the design of future few-cycle NOPCPA systems operating at the 100 TW level and beyond.

ACKNOWLEDGEMENTS This project is financially supported by the Foundation for Fundamental Research on Matter (FOM), the Netherlands Organization for Scientific Research (NWO), and the EU Integrated Initiative FP6 program Laserlab-Europe.

REFERENCES

- I.N. Ross, P. Matousek, M. Towrie, A.J. Langley, J.L. Collier, *Opt. Commun.* **144**, 125 (1997)
- T. Brabec, F. Krausz, *Rev. Mod. Phys.* **72**, 545 (2000)
- G.D. Tsakiris, K. Eidmann, J. Meyer-ter-Vehn, F. Krausz, *New J. Phys.* **8**, 19 (2006)
- G.A. Mourou, T. Tajima, S.V. Bulanov, *Rev. Mod. Phys.* **78**, 309 (2006)
- M. Geissler, J. Schreiber, J. Meyer-ter-Vehn, *New J. Phys.* **8**, 186 (2006)
- S. Witte, R.T. Zinkstok, W. Hogervorst, K.S.E. Eikema, *Opt. Express* **13**, 4903 (2005)
- V.V. Lozhkarev, G.I. Freidman, V.N. Ginzburg, E.V. Katin, E.A. Khazanov, A.V. Kirsanov, G.A. Luchinin, A.N. Mal'shakov, M.A. Martyanov, O.V. Palashov, A.K. Poteomkin, A.M. Sergeev, A.A. Shaykin, I.V. Yakovlev, S.G. Garanin, S.A. Sukharev, N.N. Rukavishnikov, A.V. Charukhchev, R.R. Gerke, V.E. Yashin, *Opt. Express* **14**, 446 (2006)
- C.P. Hauri, P. Schlup, G. Arisholm, J. Biegert, U. Keller, *Opt. Lett.* **29**, 1369 (2004)
- R.T. Zinkstok, S. Witte, W. Hogervorst, K.S.E. Eikema, *Opt. Lett.* **30**, 78 (2005)
- S. Witte, R.T. Zinkstok, A.L. Wolf, W. Hogervorst, W. Ubachs, K.S.E. Eikema, *Opt. Express* **14**, 8168 (2006)
- I.N. Ross, P. Matousek, G.H.C. New, K. Osvay, *J. Opt. Soc. Am. B* **19**, 2945 (2002)
- P. Di Trapani, A. Andreoni, G.P. Banfi, C. Solcia, R. Danielius, A. Piskarskas, P. Foggi, M. Monguzzi, C. Sozzi, *Phys. Rev. A* **51**, 3164 (1995)
- R.A. Baumgartner, R.L. Byer, *IEEE J. Quantum Electron.* **QE-15**, 432 (1979)
- L. Hongjun, Z. Wei, C. Guofu, W. Yishan, C. Zhao, R. Chi, *Appl. Phys. B* **79**, 569 (2004)
- C. Wang, Y. Leng, X. Liang, B. Zhao, Z. Xu, *Opt. Commun.* **246**, 323 (2005)
- H. Liu, W. Zhao, Y. Yang, H. Wang, Y. Wang, G. Chen, *Appl. Phys. B* **82**, 585 (2006)
- G. Arisholm, J. Biegert, P. Schlup, C.P. Hauri, U. Keller, *Opt. Express* **12**, 518 (2004)
- L. Cardoso, G. Figueira, *Opt. Express* **12**, 3108 (2004)

- 19 F. Tavella, A. Marcinkevičius, F. Krausz, *New J. Phys.* **8**, 219 (2006)
- 20 G. Cerullo, S. De Silvestri, *Rev. Sci. Instrum.* **74**, 1 (2003)
- 21 R.A. Fischer, W.K. Bischel, *J. Appl. Phys.* **46**, 4921 (1975)
- 22 W.H. Press, S.A. Teukolsky, W.T. Vetterling, B.P. Flannery, *Numerical Recipes in C* (Cambridge University Press, New York, 1992)
- 23 D. Zhang, Y. Kong, J.-Y. Zhang, *Opt. Commun.* **184**, 485 (2000)
- 24 X. Yang, Z. Xu, Z. Zhang, Y. Leng, J. Peng, J. Wang, S. Jin, W. Zhang, R. Li, *Appl. Phys. B* **73**, 219 (2001)
- 25 N. Forget, A. Cotel, E. Brambrink, P. Audebert, C. Le Blanc, A. Jullien, O. Albert, G. Chériaux, *Opt. Lett.* **30**, 2921 (2005)
- 26 L.J. Waxer, V. Bagnoud, I.A. Begishev, M.J. Guardalben, J. Puth, J.D. Zuegel, *Opt. Lett.* **28**, 1245 (2003)